A Detergent-like Mechanism of Action of the Cytolytic Toxin Cyt1A from *Bacillus thuringiensis* var. *israelensis*†

Slobodanka D. Manceva,‡ Marianne Pusztai-Carey,§ Paul S. Russo,|| and Peter Butko*,‡

Department of Chemistry and Biochemistry, University of Southern Mississippi, Hattiesburg, Mississippi 39406-5043, Department of Biochemistry, Case Western Reserve University, 10900 Euclid Avenue, Cleveland, Ohio 44106-4935, and Department of Chemistry, Louisiana State University, 242 Chopin Hall, Baton Rouge, Louisiana 70803-1804

Received July 15, 2004; Revised Manuscript Received November 3, 2004

ABSTRACT: The cytolytic δ-endotoxin Cyt1A from *Bacillus thuringiensis* var. *israelensis* is used in commercial preparations of environmentally safe insecticides. The current hypothesis on its mode of action is that the toxin self-assembles into well-defined cation-selective channels or pores, which results in colloid-osmotic lysis of the cell. Recently, a new hypothesis has been put forward suggesting that Cyt1A rather nonspecifically aggregates on the membrane surface and acts in a detergent-like manner. To distinguish between these two hypotheses, we investigated whether in the presence of lipid Cyt1A self-assembles into stoichiometric oligomers, which are characteristic of pores or channels, or aggregates into nonstoichiometric complexes, which would support the detergent-like model. Sodium dodecyl sulfate−polyacrylamide gel electrophoresis revealed that in the presence of lipid Cyt1A forms protein aggregates with a broad range of molecular weights, some being too large to enter the gel. Cyt1A tryptophan (Trp) fluorescence in the presence of lipid exhibited a decrease in anisotropy and quantum yield, but an unchanged lifetime, which is consistent with the presence of toxin aggregates in the membrane. Electrostatic interactions between the charged amino acid residues and the lipid headgroups are responsible for bringing the protein to the membrane surface, while hydrophobic and/or van der Waals interactions make the membrane binding irreversible. Fluorescence photobleaching recovery, a technique that measures the diffusion coefficient of fluorescently labeled particles, and epifluorescence microscopy revealed that upon addition of Cyt1A lipid vesicles were broken into smaller, faster diffusing objects. Since no change in size or morphology of the vesicles is expected when pores are formed in the osmotically equilibrated membranes, our results support the detergent-like mode of action of Cyt1A.

Bacillus thuringiensis var. *israelensis* (Bti)[1] are spore-forming Gram-positive bacteria, which during the stationary phase of the bacterial growth form parasporal inclusion bodies containing δ-endotoxins. These toxins are historically divided into two groups: Cry and Cyt. While the mechanism of action of Cry proteins has been determined (*1*, *2*), the mechanism of action of Cyt proteins remains a subject of controversy.

The current hypothesis of the Cyt1A mode of action is colloid-osmotic lysis (*3*). Ellar and co-workers based this hypothesis on observations made in the last 20 years. Initially, Thomas and Ellar observed that when solubilized Bti crystals were applied to the cells derived from *C. fumiferana* (Eastern spruce budworm) 63 CFI or *A. albopictus* (Asian tiger mosquito), the cells were destroyed (*4*). Further studies suggested that the cytolytic δ-endotoxins from Bti may form pores or channels in the plasma membrane through which ions can equilibrate, inducing an influx of water and a subsequent swelling of the cell, leading to the eventual cell lysis (*3*). Experiments with planar lipid bilayers (*5*) supported that notion. According to this hypothesis the toxin forms cation-selective channels or pores, which mediate the colloid-osmotic lysis of epithelial cells in the insect gut, eventually killing the insect by starvation.

However, some data do not conform to the pore-forming or colloid-osmotic lysis hypothesis [reviewed by Butko (*6*)]. We suggest that, at least in vitro, the Cyt toxins may act in a less specific "detergent-like" manner, as originally considered by Thomas and Ellar (*4*, *7*). According to this hypothesis, the toxin adsorbs onto the membrane surface, where it nonspecifically aggregates into large carpet-like structures, which destabilize the membrane and cause defects in the lipid packing, through which the cytoplasm can leak out from the cell. Eventually the lipid membrane is broken up into micellar protein−lipid complexes, and the cell is completely disintegrated.

† This research was supported by the Cooperative State Research, Education, and Extension Service, U.S. Department of Agriculture (agreement number 2001-35302-1011138) and by the National Science Foundation (Grant DMS-0241236).

* Corresponding author. Tel: 601-266-6044. Fax: 601-266-6075. E-mail: peter.butko@usm.edu.

‡ University of Southern Mississippi.

§ Case Western Reserve University.

|| Louisiana State University.

[1] Abbreviations: Bti, *Bacillus thuringiensis* var. *israelensis*; DC, direct current; FPR, fluorescence photobleaching recovery; GUV, giant unilamellar vesicles; HEPES, *N*-(2-hydroxyethyl)piperazine-*N*′-2-ethanesulfonic acid; LUV, large unilamellar vesicles; NBD-PC, 1-acyl-2-[12-[(7-nitro-2,1,3-benzoxadiazol-4-yl)amino]dodecanoyl]-*sn*-glycero-3-phosphocholine; PAGE, polyacrylamide gel electrophoresis; PC, egg L-α-phosphatidylcholine; RFRET, relative change in the fluorescence resonance energy transfer; SDS, sodium dodecyl sulfate; SUV, small unilamellar vesicles.

10.1021/bi048493y CCC: $30.25
Published on Web 12/22/2004

We have previously shown that Cyt1A, considered here a representative of the entire Cyt family, increases its surface hydrophobicity with a decrease in the pH, thereby increasing its affinity toward the lipid (*8*). Questions we address in the present work are as follows: Does Cyt1A self-assemble into well-defined proteinaceous pores or rather nonstoichiometric aggregates? What forces dominate the toxin−lipid interactions? What is the effect of the toxin on the size and morphology of the model membranes in osmotic equilibrium? Results obtained with a variety of biochemical and biophysical experiments support the detergent-like mode of Cyt1A action rather than pore forming.

EXPERIMENTAL PROCEDURES

Materials. Egg L-α-phosphatidylcholine (PC) was purchased from Sigma-Aldrich (St. Louis, MO), and the 1-acyl-2-[12-[(7-nitro-2,1,3-benzoxadiazol-4-yl)amino]dodecanoyl]-*sn*-glycero-3-phosphocholine (egg-transphosphatidylated, chicken) (NBD-PC) was obtained from Avanti Polar Lipids, Inc. (Alabaster, AL). Tris/glycine/sodium dodecyl sulfate (SDS) 4−20% gradient gels, the 2× sample buffer, and the Tris/SDS/HEPES running buffer were from VWR (Atlanta, GA). Molecular weight standards (Mark 12) were from Invitrogen (Carlsbad, CA). GelCode Blue Stain and the bicinchoninic acid (BCA) protein assay kit were from Pierce (Rockford, IL). All the other buffers and salts were from VWR (Atlanta, GA) or Fisher Scientific (Pittsburgh, PA).

Purification of Cyt1A. The toxin Cyt1A was purified from cultures of *Bacillus thuringiensis* var. *israelensis* (natural strain) as previously described (*9*). In short, the bacteria were lysed, and the parasporal crystals were separated and solubilized in 10 mM dithiothreitol (DTT) and 50 mM Na_2CO_3/HCl, pH 9.5. The Cyt1A protoxin was purified using high-performance liquid chromatography (HPLC) on a mono-Q ion-exchange column (Pharmacia LKB, Uppsala, Sweden) with a linear gradient of 10−800 mM NH_4HCO_3, pH 8.5 (*10*). The protoxin was activated by tryptic digestion. The purity of the preparation was routinely checked by sodium dodecyl sulfate−polyacrylamide gel electrophoresis (SDS−PAGE). The purified toxin was lyophilized and stored at −20 °C.

Preparation of Model Membranes. Small unilamellar vesicles (SUV) were prepared by sonication as previously described (*8*). In short, 5 mg of lipid in chloroform was dried under a stream of nitrogen. The resulting thin film was hydrated in 0.5 mL of buffer containing 10 mM HEPES and 100 mM NaCl, pH 7.4. The lipid suspension was sonicated for 30 min at 4 °C with a Sonic Dismembrator Model 300 (Fisher Scientific, Pittsburgh, PA).

Large unilamellar vesicles (LUV) were prepared by extrusion as previously described (*9*): the aqueous lipid suspension was vortexed, frozen and thawed twice, and extruded 21 times through a stack of two polycarbonate membranes with a 100 nm pore, using a LiposoFast extruder (Avestin Inc., Ottawa, Ontario, Canada). Fluorescently labeled LUV (NBD-PC LUV) were prepared in the same way except that the lipid contained 5 mol % NBD-PC.

Giant unilamellar vesicles (GUV) were prepared using the procedure described by Moscho et al. (*11*). In short, 1.9 mg of PC and 0.1 mg of NBD-PC in chloroform were added to 1 mL of a 6.5:1 mixture of $CHCl_3$ and CH_3OH in a 50 mL round-bottom flask. The aqueous phase (7.0 mL of 10 mM HEPES, 150 mM NaCl, pH 7.4, buffer) was carefully added along the flask walls. After the organic solvent was removed by evaporation under reduced pressure, an opalescent fluid containing a high concentration of GUV was obtained.

Relative Change in the Fluorescence Resonance Energy Transfer (*RFRET*). RFRET was obtained by measuring the fluorescence of 1.0 μM Cyt1A when tyrosine (Tyr) residues are preferentially excited at 260 nm (F_{260}) and when tryptophan (Trp) residues are exclusively excited at 295 nm (F_{295}). The ratio of tryptophan fluorescence intensities with excitations at 260 and 295 nm, $r_1 = F_{260}/F_{295}$, is proportional to the efficiency of the resonance energy transfer between Tyr and Trp residues in a given conformation of the protein. When the conformation changes, the fluorescence ratio F_{260}/F_{295} is likely to change since the efficiency of the resonance energy transfer is a steep function of the distance between, and orientation of, the fluorescent amino acid residues. Thus the ratio R of relative fluorescence after and prior to the conformation change, $R = r_2/r_1$, can be used to infer the magnitude of the conformation change in the protein, brought about by any experimental interference (a change in pH or salt concentration, addition of lipid, etc.). This technique is useful for a rapid determination whether an experimental treatment results in a conformation change in the protein or not. Even in the case of multiple tyrosine and tryptophan residues in the protein, one can still detect an overall global conformation change, as was previously demonstrated (*12*). A drawback of the RFRET technique, especially in the case of multiple Tyr and Trp, is that it does not provide information on the nature and location of the conformation change. Detailed assessment of using RFRET to determine overall conformation changes in protein is beyond the scope of this paper and will be addressed separately. Steady-state fluorescence spectra of Cyt1A with either 260 or 295 nm excitation were recorded with an ISS PC1 (Champaign, IL) photon-counting fluorometer. Excitation and emission slits were 8 nm. Data were corrected for dilution and, in the presence of lipid, also for light scattering.

Fluorescence Lifetime Measurements. A phase-and-modulation fluorometer ISS K2 (Champaign, IL), equipped with a xenon lamp, variable slits, and microprocessor-controlled photomultiplier gain, was used to determine fluorescence lifetime in the frequency domain [see, e.g., Lakowicz (*13*)]. Experimental data of phase ϕ_ω and modulation m_ω as a function of modulation frequency of the excitation were fitted with the equations

$$\tan \phi_\omega = \omega\tau \quad (1)$$

$$m_\omega = (1 + \omega^2\tau^2)^{-1/2} \quad (2)$$

from which fluorescence lifetime τ was determined. An excitation wavelength of 280 nm and 16 nm excitation and emission slits were used. Measurements were performed at 10 different logarithmically increasing frequencies, starting from 2 and ending at 250 MHz. Samples (in 10 × 10 mm or 3 × 3 mm quartz cuvettes) contained 1.0 μM Cyt1A in the presence or absence of 150 μM PC (in the form of SUV). Lifetime was measured in three independent experiments, and the mean ± standard error is reported.

SDS−PAGE Gel Electrophoresis. SDS−PAGE was conducted as described by Promdonkoy and Ellar (*14*). Purified

Cyt1A was solubilized in 10 mM NH_4HCO_3, pH 8.5. Toxin samples (10 μM) were incubated with lipid (osmotically balanced PC LUV) in 10 mM HEPES and 150 mM NaCl, pH 7.4, for 1 h at room temperature. Toxin:lipid ratios were 1:50, 1:150, or 1:500. Incubation was stopped by addition of the 2× sample buffer. Protein samples were loaded onto a 4−20% gradient gel without boiling, and electrophoresis was carried out at 150 V for 90 min at room temperature. Mark 12 was used as a protein molecular weight marker set. Bands were visualized by the GelCode Blue Stain.

In experiments with increasing ionic strength, Cyt1A was incubated for 60 min in the presence or absence of lipid in 10 mM HEPES, pH 7.4, and 0, 0.1, or 1.0 M NaCl. The toxin:lipid molar ratio was 1:150. Incubation was stopped by addition of the 2× sample buffer, and the samples were subjected to electrophoresis.

Reversibility of the lipid binding was tested in experiments where the toxin was first allowed to bind to the lipid and ionic strength was increased afterward. Cyt1A was incubated with LUV, at the same toxin:lipid ratio as above, in 0.1 M NaCl for 1 h at room temperature. Subsequently, additional salt was added up to 1.5 M, and the samples were incubated for another 30 min. After addition of the 2× sample buffer, the toxin aggregates were resolved by using SDS−PAGE as described above.

Fluorescence Photobleaching Recovery (*FPR*). FPR is a technique that measures the diffusion rate of fluorescently labeled particles. A home-built instrument (located at Louisiana State University, Baton Rouge, LA) was employed. Details of the technique and its attributes, especially compared to dynamic light scattering, and the experimental setup are described in Fong et al. (*15*). Briefly, a bright laser flash illuminates the stationary amplitude gradient (Ronchi ruler), which is placed in the rear image plane of a standard epifluorescence microscope. Photobleaching creates a dark striped pattern in the sample. The pattern fades due to the diffusion of the particles from the nonbleached area to the bleached area of the image. Moving the Ronchi ruler in and out of phase with the bleached image enhances detection of the small contrast changes in the image. This motion produces a weak triangular wave ripple on the top of the large DC signal, detected by the photomultiplier. The ripple represents the pattern written into the sample, and the DC represents the overall fluorescence intensity in the illuminated region. With the recovery of the fluorescence in the bleached parts, the triangular wave fades, and the kinetics of the fading is used to determine the mutual diffusion coefficient of the fluorescent particles.

In our case, fluorescent diffusers were 5% NBD-labeled PC LUV (300 nM) lipid. They were incubated with increasing concentrations (from 0.05 to 1.6 μM) of Cyt1A for 15 min at room temperature. Aliquots of each sample were placed into rectangular capillary tubes (Vitro Com, Inc., Mt. Lakes, NJ) and bleached for 0.5 s with a 488 nm laser pulse (Lexel Model 95 Ar^+, power of up to 2 W at 488 nm). Recovery of the fluorescence in the bleached samples was monitored at 25.0 ± 0.1 °C by photomultiplier tubes RCA7265. Data were analyzed using the AnScan software developed in P. S. Russo's laboratory at Louisiana State University and CONTIN. Changes in the apparent hydrodynamic radius of the labeled lipid particles were calculated from the experimental values of the optical tracer self-diffusion coefficient D_s, using the Stokes−Einstein equation:

$$R_{h,app} = kT/(6\pi\eta_0 D_s) \quad (3)$$

where k is the Boltzmann constant, T the absolute temperature, and η_0 the solvent viscosity.

Epifluorescence Microscopy. Increasing amounts of Cyt1A (concentrations 2.8−8.5 μM) were added to 3 μL of the 5% NBD-labeled PC GUV (5 mM) suspension and incubated for 15 min at room temperature. Images were collected with a fluorescence microscope (Olympus BX60, Tokyo, Japan) equipped with a digital camera (Imaging-MicroPublisher, Burnaby, British Columbia, Canada) and processed with Photoshop 6.0 (Adobe Systems, Mountain View, CA).

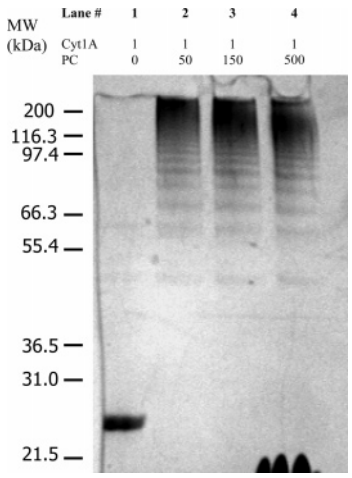

FIGURE 1: Aggregation of Cyt1A in the presence of PC LUV. Cyt1A was incubated with an increasing concentration of lipid for 1 h at room temperature. Incubation was stopped by addition of the 2× SDS/glycine sample buffer (4% SDS, glycerol, 0.01% Bromophenol blue, 0.125 M Tris-HCl, β-mercaptoethanol), and samples were immediately loaded onto a 4−20% gradient Tris/glycine/SDS gel. Toxin:lipid molar ratios were 1:0 (lane 1), 1:50 (lane 2), 1:150 (lane 3), and 1:500 (lane 4).

RESULTS

Cyt1A on the Lipid Membrane: Aggregates or Self-Assemblies? (A) SDS−PAGE. SDS−PAGE analysis of Cyt1A has the potential to distinguish between pore formation and detergent-like mode of action: if in the presence of lipid Cyt1A self-assembles into SDS-insoluble protein-lined pores, a protein band with a molecular weight of the oligomeric pore should appear, possibly accompanied by a few weaker bands at lower molecular weights corresponding to incomplete pores or intermediate aggregates. This has been observed with, for example, the poliovirus 2B protein (*16*). On the other hand, if the toxin in the presence of lipid forms nonstoichiometric aggregates, then protein bands with a broad distribution of molecular weights are expected, with no limits in molecular weight, at least in principle. Figure 1 represents Cyt1A bands in the absence (lane 1) and presence of increasing amounts of lipid (toxin:lipid molar ratios of 1:50, 1:150, and 1:500, lanes 2, 3, and 4, respectively). In the absence of lipid Cyt1A migrated in the gel as a monomer; the faint band at molecular weight 48000 is attributed to the Cyt1A dimer, which is the native species in aqueous solution. In the presence of lipid the Cyt1A bands formed a laddering pattern with distribution of molecular weights from small

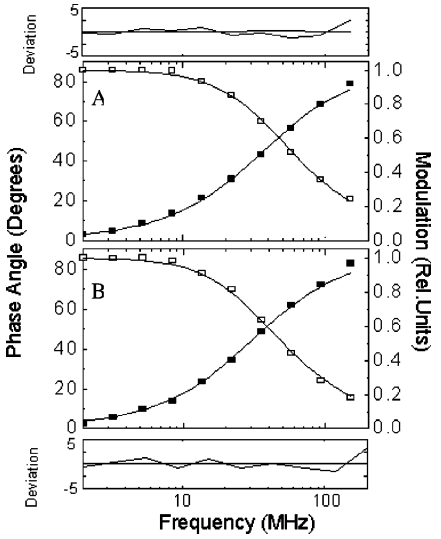

FIGURE 2: Cyt1A fluorescence lifetime. Phase (■) and modulation (□) data with a discrete exponential fit and residuals (difference between the data and the fit) as functions of modulation frequency in the absence (A) and presence (B) of lipid (PC SUV). Toxin and lipid concentrations were 1 and 150 μM, respectively.

oligomers to large polymers, some of the latter being so large that they could not enter the gel. The size of the aggregates appears to decrease with a decreasing toxin:lipid molar ratio. It is important to note that the toxin aggregates were stable in the presence of high concentrations of SDS in the gel. The aggregates dissociated when samples were boiled before loading on the gel; in that case the entire toxin migrated as a monomer (data not shown).

(B) Fluorescence Lifetime Measurements. A 50% decrease in fluorescence intensity in the presence of lipid was reported previously (*8*). This decrease was not accompanied by a significant red shift in the fluorescence maximum, which normally is observed if the environmentally sensitive Trp residues are more exposed to the polar (aqueous) environment. To gain more insight into the lipid-induced quenching of Trp fluorescence, we measured the effect of lipid on the fluorescence lifetime. Figure 2 shows the phase and modulation data with a discrete exponential fit and residuals (difference between the data and the fit) as a function of modulation frequency. We found that the two Trp residues in strand 4 of the Cyt1A predicted structure (*6*) exhibited a single discrete lifetime of 4.40 ± 0.08 ns (Figure 2A), and the addition of lipid did not affect that value (4.50 ± 0.15 ns; Figure 2B).

Forces Involved in the Cyt1A Interaction with Lipids. (A) SDS−PAGE. Increasing ionic strength shields electrostatic charges and decreases electrostatic forces. To test the involvement of electrostatic forces in the Cyt1A−membrane interaction, we again employed SDS−PAGE and fluorescence spectroscopy. Figure 3A shows results of the experiment testing the effect of ionic strength on the Cyt1A−lipid interaction. Lanes 1, 3, and 5 represent the toxin incubated in the absence of lipid with 0.0, 0.1, and 1.0 M NaCl, respectively. The toxin migrated as one band with an approximate molecular weight of 24000. The samples in lanes 2, 4, and 6 are Cyt1A incubated with PC LUV at a toxin:lipid molar ratio of 1:150, with 0.0, 0.1, and 1.0 M NaCl, respectively. The results demonstrate that an increasing ionic strength inhibited formation of the lipid-induced Cyt1A aggregates. The diminished staining at high molecular weight is especially conspicuous at 1 M salt (lane 6), where also the monomer band is clearly apparent.

If electrostatic forces were the only ones to keep the toxin bound to the membrane, one would expect dissociation of the bound toxin upon increase of the ionic strength. Therefore, we performed an experiment where Cyt1A was preincubated with PC LUV at 0.1 M NaCl for 60 min at room temperature and then the ionic strength was increased by adding NaCl to a final concentration of 0, 0.25, 0.5, 1.0, or 1.5 M (Figure 3B, lanes 2, 3, 4, 5, and 6, respectively). After an additional incubation for 30 min at room temperature, Cyt1A aggregates were resolved on a 4−20% gradient Tris/glycine/SDS gel. The gel shows that an increased ionic strength did not have any effect on Cyt1A after preincubation of the toxin with lipid.

(B) Relative Fluorescence Resonance Energy Transfer (*RFRET*). Lipid-induced changes in RFRET between Tyr and

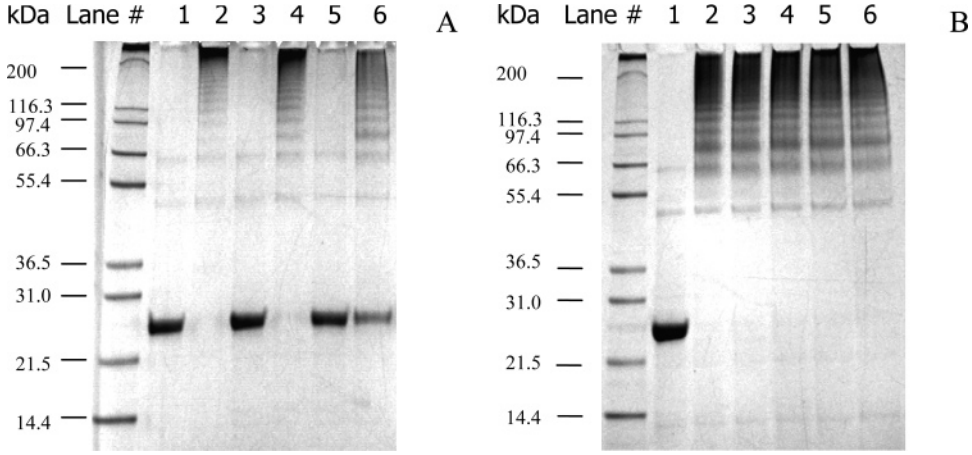

FIGURE 3: (A) Effect of increasing ionic strength on Cyt1A:lipid interaction. Ten micromolar Cyt1A was incubated without (lanes 1, 3, and 5) or with 1.5 mM PC LUV (lanes 2, 4, and 6) in 10 mM HEPES and 0.0 (lanes 1 and 2), 0.1 (lanes 3 and 4), or 1.0 (lanes 5 and 6) M NaCl, pH 7.4, for 60 min at room temperature. Nonboiled samples were resolved on 4−20% Tris/glycine/SDS gradient gels and stained with GelCode Blue Stain. (B) Effect of increasing ionic strength on Cyt1A interacted with lipid. Ten micromolar Cyt1A was incubated without (lane 1) or with (lane 2) 1.5 mM PC in 10 mM HEPES and 0.1 M NaCl, pH 7.4, for 60 min at room temperature. We attempted to remove the bound protein by addition of 0.25, 0.5, 1.0, and 1.5 M NaCl (lanes 3−6, respectively) followed by further incubation at room temperature for 30 min. Nonboiled samples were resolved on 4−20% Tris/glycine/SDS gradient gels and stained with GelCode Blue Stain.

Table 1: Effect of Ionic Strength on the Cyt1A Interaction with PC SUV[a]

[NaCl] (M)	r_1 (Cyt1A)	r_2 (Cyt1A + PC)	RFRET ($R = r_2/r_1$) Cyt1A	RFRET ($R = r_2/r_1$) Cyt1A + PC
0.0	0.557 ± 0.003	0.391 ± 0.006	1.00 ± 0.00	0.70 ± 0.02
0.1	0.557 ± 0.003	0.498 ± 0.006	1.00 ± 0.00	0.89 ± 0.02
1.0	0.563 ± 0.007	0.512 ± 0.006	1.00 ± 0.01	0.92 ± 0.02

[a] Fluorescence spectra were collected when Tyr and Trp residues were exclusively excited at 260 and 295 nm. The ratio of fluorescence intensities for each excitation wavelength ($r = F_{260nm}/F_{295nm}$) is proportional to the efficiency of fluorescence resonance energy transfer between Tyr and Trp at 0.0, 0.1, and 1.0 M NaCl. The ratio $R = r_2/r_1$ is then the relative change in the energy transfer, denoted RFRET. Protein and lipid concentrations were 1.0 μM and 1.0 mM, respectively. Columns 4 and 5 represent the normalized data to the ratios of the fluorescence maxima in the absence of lipid.

Table 2: Effects of Ionic Strength and Lipid on Steady-State Fluorescence Anisotropy of Cyt1A[a]

[NaCl] (M)	r (Cyt1A)	r (Cyt1A + PC)
0.0	0.128 ± 0.001	0.107 ± 0.002
0.1	0.128 ± 0.001	0.110 ± 0.002
1.0	0.131 ± 0.002	0.120 ± 0.002

[a] The samples contained 1 μM Cyt1A, 0, 0.1, or 1.0 mM NaCl, and 1.0 mM PC SUV (if present). The excitation wavelength was 280 nm. The values with the standard errors are averages of 10 determinations.

Trp residues were determined from Trp fluorescence intensities measured at two excitation wavelengths, 260 nm, which preferentially excites Tyr, and 295 nm, which exclusively excites Trp. In both cases only Trp fluorescence is observed because the energy of the Tyr residues is readily transferred to the Trp residues present. A change in the ratio of the two fluorescence intensities upon the addition of lipid represents the relative change in the energy transferred from Tyr to Trp, brought about by binding to the lipid.

We measured the RFRET in the presence and absence of PC SUV and at different ionic strengths. Data are given in Table 1. The fluorescence ratio F_{260}/F_{295} appears to be independent of the NaCl concentration in the absence of lipid. In the presence of lipid at 0 M NaCl a 30% decrease in FRET is observed, but only an 8% decrease is caused by lipid at 1.0 M NaCl.

(C) Steady-State Fluorescence Anisotropy. Values of fluorescence anisotropy of Cyt1A in the presence and absence of lipid at different salt concentrations are shown in Table 2. It is apparent that the values followed the same trend as the one observed in the RFRET experiment. Namely, binding to the lipid caused a decrease in Cyt1A fluorescence anisotropy, and the decrease was attenuated at a high ionic strength. In the absence of lipid, the anisotropy remained constant, about 0.128.

Size and Morphology of Model Membranes in the Presence of Cyt1A. (A) Fluorescence Photobleaching Recovery. Figure 4 shows size distribution of fluorescently labeled PC LUV as calculated from FPR data. In the absence of Cyt1A, a well-defined uniform population of NBD-labeled PC LUV (filled squares) with an apparent hydrodynamic radius ($R_{h,app}$) of 60 nm was observed. This is consistent with the nominal size of the LUV that were prepared by extrusion through filters with 100 nm pores. Upon addition of 100 nM Cyt1A (open circles), three populations of fluorescent diffusers were

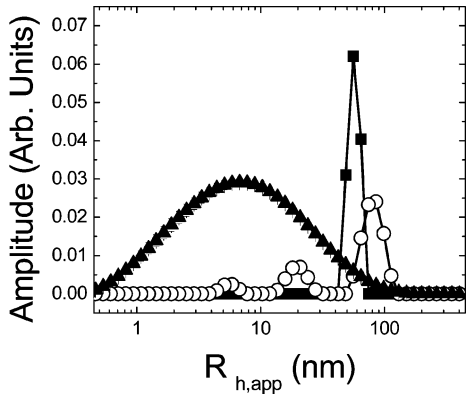

FIGURE 4: Size distributions of NBD-labeled lipid vesicles. PC LUV (300 nM) with $R_{h,app}$ of 60 nm in the absence (squares) and presence of 100 nM Cyt1A (circles) and upon addition of 0.1% Triton X-100 (triangles). Data were normalized for the area under the curve. Fitting errors were smaller than the size of the symbols.

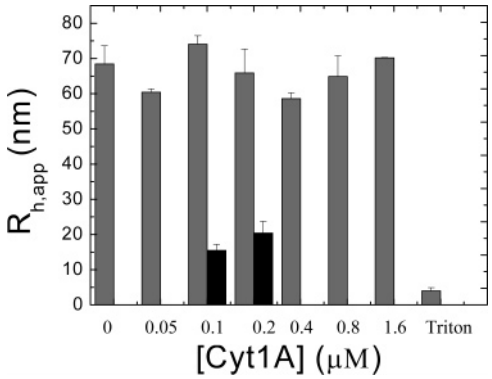

FIGURE 5: Effect of Cyt1A on the mean hydrodynamic radius $R_{h,app}$ of NBD-labeled PC LUV (300 nM lipid). The bars represent fitting errors from CONTIN.

observed, with apparent hydrodynamic radii of 80, 20, and 6 nm, respectively. Upon addition of detergent (0.1% Triton X-100, triangles) a very broad distribution of diffusers with an average $R_{h,app}$ of 7 nm was observed. This experiment was repeated three times, and Figure 4 shows representative results.

The concentration dependency of these effects was tested with an increasing concentration of Cyt1A from 0 to 1.6 μM (Figure 5). A population of smaller, faster diffusers appeared at 0.1 and 0.2 μM toxin (filled bars); however, higher toxin concentrations, up to 1.6 μM, resulted in a single population of larger diffusers with an $R_{h,app}$ of about 65 nm. Addition of a 0.1% (v/v) nonionic detergent, Triton X-100, resulted in a broad distribution of diffusers with an average $R_{h,app}$ of 7 nm.

(B) Epifluorescence Microscopy. It was puzzling that the population of small diffusers disappeared at higher toxin concentrations (Figure 5). We suspected that this might be due to coalescing or aggregation of the smaller toxin−lipid complexes that remained from the broken up LUV. Although the size of the aggregates might be similar to that of the intact LUV, their morphology might be different. To visualize the effect of the toxin on the lipid vesicles, we used epifluorescence microscopy of NBD-labeled GUV. Figure 6 shows fluorescence micrographs of the lipid vesicles in the absence (A1, B1, and C1) and presence of Cyt1A (A2 to A4 and B2 to B5) or the nonionic detergent Triton X-100 (A5, B5, and C2 to C5). The change in the morphology of

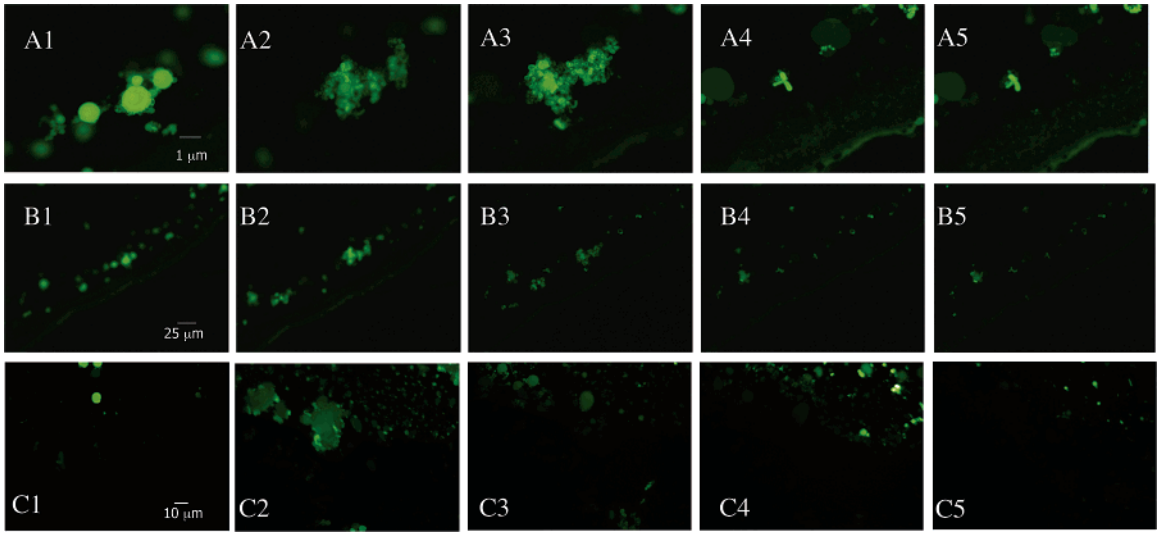

FIGURE 6: Epifluorescence micrographs of NBD-labeled PC GUV in the absence or presence of Cyt1A and Triton X-100. Panel A: A sequential increase in Cyt1A concentration (0, 2.8, 5.7, 8.5 μM, A1−A4, respectively) plus the addition of 0.1% Triton X-100 (A5). Panel B: A broader view of the micrographs in panel A. Panel C: A sequential increase in Triton X-100 concentration [0, 0.007%, 0.014%, 0.021%, and 0.028% (v/v)].

the lipid vesicles is obvious with the addition of either the toxin (2.8 μM) or the detergent [0.01% (v/v)], as shown in panels A2 or C2, respectively. With further addition of toxin (5.7 μM, panel A3), the vesicles were destroyed. The small protein−lipid complexes coalesced together. The overall size of the clusters was similar to that of the intact GUV. At 8.5 μM Cyt1A all of the toxin−lipid complexes were destroyed (very small fluorescent particles can be seen at the bottom of panel A4); addition of 0.1% (v/v) Triton X-100 did not have any further effect on the size of toxin−lipid complexes, suggesting that they were in a micellar form (A5). Micrographs in panel B represent a broader view of the same field as in panel A, to show that the toxin effect is not localized but all vesicles are affected. This experiment was performed twice with similar results. A conclusion can be drawn that, qualitatively, the damages inflicted upon the lipid vesicles by Cyt1A are very similar to those caused by detergent.

DISCUSSION

Self-Assembly or Aggregation. The leading hypothesis of Cyt1A mode of action, formulated by Ellar and co-workers (*3*−*5*, *7*, *14*, *17*−*20*), is that toxin monomers bind and insert into the cell membrane, where they self-assemble into β-barrel cation-selective channels or pores with a diameter of 1−2 nm. However, this hypothesis does not easily explain some experimental data (*8*, *9*). We put forward an alternative hypothesis, according to which Cyt1A aggregates on the membrane surface without a substantial membrane penetration or stoichiometric structures; the aggregates destabilize the cell membrane and break it up in a detergent-like manner (*6*). In the present work we specifically tested if Cyt1A self-assembles into a well-defined stoichiometric pores or rather aggregates in nonstoichiometric structures. If Cyt1A self-assembles into well-defined β-barrel protein-lined pores, the assemblies will contain a stoichiometric number of protein units forming the pore. According to the pore-forming hypothesis, that number is six (*2*, *19*, *20*). Such protein assemblies should be easily resolved by gel electrophoresis: provided the assemblies are SDS-stable, a predominant protein band in gels should be that of a hexamer (144 kDa). Such oligomers were experimentally observed with known pore-forming toxins: α-hemolysin, which forms heptameric pores (*21*), and the 2B protein produced by enterovirus, which self-assembles into tetrameric pores (*16*). However, if the toxin aggregates into a "carpet" of a nonspecific size, the Cyt1A in the gel would exhibit a laddering pattern or "smear" with bands corresponding to monomers, dimers, trimers, etc., to unresolvable polymers of high molecular mass.

As Figure 1 shows, in the presence of lipid a laddering pattern of toxin bands with molecular masses between 48 kDa and infinity was observed. Although the mean molecular mass of the aggregates decreased with the toxin:lipid molar ratio decreasing from 1:50 (lane 2) to 1:500 (lane 4), large protein aggregates that could not enter the gel were present in all cases. Another important characteristic of the lipid-induced aggregates is the resistance to SDS, which was first observed by Promdonkoy and Ellar (*14*). Samples used in this experiment were not boiled before loading, and the aggregates were not dissolved by the 1% SDS contained in the Tris/glycine gels. This suggests that the toxin aggregates are so tight that the SDS molecules could not intercalate into them and that, apart from hydrophobic interactions, other forces such as electrostatic and van der Waals are involved.

Fluorescence spectroscopy also was employed to distinguish between self-assembly and aggregation of Cyt1A. Previously, a 50% decrease in Cyt1A fluorescence intensity was observed in the presence of lipid (*8*). The lipid-induced decrease in the fluorescence quantum yield may have two causes: (i) collisional quenching by polar solvent molecules due to the higher exposure of the two Trp residues to the aqueous environment or (ii) static quenching, brought about by the closely opposed Trp residues in Cyt1A aggregates in the membrane. To distinguish between these two possibilities, we measured the lifetime of the Trp fluorescence in the absence and presence of lipid. If Trp residues became more exposed to the solvent, collisional quenching would shorten the fluorescence lifetime. If Cyt1A aggregated instead, static quenching would result in no change in the Trp fluorescence lifetime. The lifetime of Cyt1A fluorescence was 4.40 ± 0.08

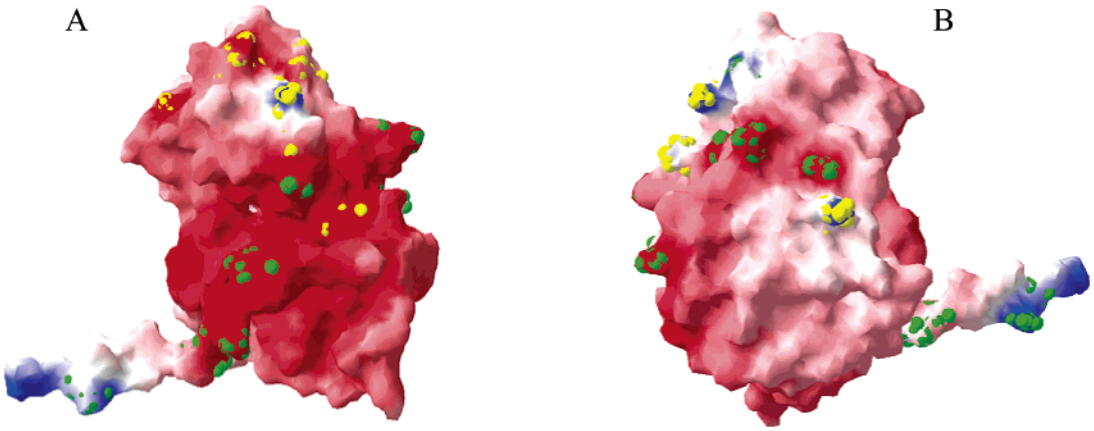

FIGURE 7: Surface electrostatic potential map of Cyt1A. Blue represents positive and red negative potential. Panel B shows the molecule rotated 180° around the vertical axis. Dysfunctional and benign amino acid mutations introduced by Ward et al. (*17*) are represented within the Cyt1A predicted structure (*6*) in yellow and green, respectively.

ns, regardless of the presence of lipid. Thus, the lipid-induced changes in Cyt1A fluorescence intensity are not due to collisional quenching. The observed decrease in fluorescence anisotropy, which may be due to resonance energy transfer, is consistent with the possible existence of nonfluorescent tryptophans (or its complexes) in closely opposed toxin molecules. Fluorescence of tryptophan in proteins can be quenched by, e.g., protonated amines, guanidinium, imidazolium, and phenyl or carboxyl groups (*13*). The predicted structure of Cyt1A (*6*) indicates that as many as 16 amino acids possessing one of the listed groups are within 12 Å of either of the two tryptophans. Several potentially quenching amino acid residues, Arg30, Phe73, Glu156, Glu164, and Lys203, are within 5 Å. It is possible that the lipid-induced conformational change brings more of these amino acids closer to either of the tryptophans, thus causing static quenching of Cyt1A fluorescence.

Tryptophan is known to exhibit two fluorescence lifetimes (*13*). Our inability to resolve them might be the consequence of technical limitations of our setup (use of a xenon lamp instead of a laser and a significant loss of intensity in the Pockels cell that modulates the excitation light) and, in part, of the inherent difficulty of measuring fluorescence in the presence of lipid vesicles. Values of χ^2 for single-exponential fits to three independent replicate data sets were between 17 and 32 and did not significantly decrease in two-exponential fits; the latter usually converged to one exponential (not shown). While our lifetime data may not have sufficient resolution for a rigorous discussion of tryptophan photophysics in Cyt1A, the main point of our argument remains valid: fluorescence lifetime of Cyt1A does not change upon addition of lipid.

Our results indicate that binding to the lipid induces nonstoichiometric aggregation of Cyt1A. Sensitivity to ionic strength suggests that electrostatic interaction between the charged lipid headgroups and charged amino acids on the Cyt1A surface plays a role in lipid binding. As is shown in Figure 3A, an increase in ionic strength attenuated the Cyt1A−lipid interaction (lanes 2, 4, and 6). Two factors may contribute to this effect: a conformation change in Cyt1A induced by the high ionic strength, which may lead to a decreased affinity toward the lipid, and simple shielding of the electrostatic interaction between Cyt1A and the lipid headgroups. Since we previously observed no changes in Cyt1A fluorescence with ionic strength between 0.15 and 2 M (*22*), we conclude that the latter is the case and, consequently, electrostatic interactions are important for the initial binding of Cyt1A to the membrane rather than for oligomerization of the toxin itself.

The RFRET data corroborate the above conclusions. Cyt1A contains six Tyr (at positions 51, 100, 171, 173, 189, and 217) and two Trp (158 and 161) residues (Figure 4). Due to the closest proximity of certain Tyr and Trp, most probable donor/acceptor pairs are Tyr171/Trp158 and Tyr173/161. Therefore, the RFRET changes most probably reflect conformation changes in and between strands 4 and 5 in the predicted structure of Cyt1A (*6*), although the precise localization of the conformation changes is not necessary for drawing the conclusion. The lipid binding caused a conformation change in Cyt1A, which resulted in a 30% decrease in FRET between Tyr and Trp, and this decrease was inhibited by high salt (Table 1). At a high ionic strength most of the toxin was not bound to the lipid: the RFRET data indicated that it was in a conformation close to the one observed in the absence of lipid.

The third confirmation of a diminished binding to the lipid at high ionic strength comes from fluorescence anisotropy data (Table 2). Increasing ionic strength resulted in an increase in the anisotropy from 0.107 (0.0 M NaCl) to 0.120 (1.0 M NaCl) in the presence of lipid, while it did not have any effect on the protein in the absence of lipid (in which case $r = 0.129$).

All of the above data confirm that electrostatic forces play an important role in the Cyt1A−membrane interactions. The amino acids that are the possible candidates for direct electrostatic interactions with the lipid headgroups can be identified with the help of the extensive mutagenesis study of Cyt1A by Ward et al. (*18*). When the following charged amino acids were mutated to neutral Ala residues, the toxin lost its activity: four (Lys124, Lys154, Lys164, and Lys203) out of the six Lys, two (Asp213 and Asp240) out of eight Asp, one (Arg78) out of the three Arg, and three (Glu45, Glu164, and Glu204) out of eight Glu residues. Ward's mutations are indicated in the toxin's surface electrostatic potential map in Figure 7. The fact that the bound Cyt1A cannot be dissociated from the membrane by increasing ionic strength (Figure 3B, lanes 2−6) indicates the involvement of nonelectrostatic forces (hydrophobic, van der Waals). In

summary, the membrane-bound Cyt1A forms nonstoichiometric aggregates with a broad range of molecular weights. Electrostatic forces between the charged Lys, Asp, Arg, and Glu residues and the lipid headgroups seem to be responsible for initial binding of the toxin to the membrane surface. Upon binding, Cyt1A changes conformation due to, at least in part, the lower local pH and becomes more hydrophobic. The second phase of the toxin−lipid interaction, involving hydrophobic and/or van der Waals forces, makes the toxin−lipid binding irreversible.

Size and Morphology of Model Lipid Membranes in the Presence of Cyt1A. We further addressed a closely related question of the size of the toxin−lipid aggregates. Depending on conditions, peptide toxins either form small pores or channels at relatively low concentrations [e.g., alamethicin (*23*)], form large polymeric pores [e.g., cholesterol dependent cytolysins (*24*)], or perturb the membrane by a mechanism termed the carpet model, proposed by Shai (*23*). The latter mechanism is characterized by accumulation of large peptide aggregates on the membrane surface without significant penetration into the core of the lipid bilayer. Only at high surface concentration are some peptide molecules forced to insert into the bilayer, which leads to destabilization of the membrane. We hypothesized that, in the final stage of such a toxin action, the membrane is broken up into smaller toxin−lipid complexes (*6*).The present results validate that hypothesis: FPR of fluorescently labeled LUV revealed that a population of faster, smaller fluorescent diffusers, referred to as toxin−lipid complexes, appears in the presence of Cyt1A. An interesting puzzling detail, namely, that at higher toxin concentrations only a slow diffusing population was observed with $R_{h,app}$ not much different from that of the LUV in the absence of the toxin (Figure 5), was resolved by epifluorescence microscopy images of the fluorescently labeled GUV: the small lipid−toxin complexes, resulting from the break up of the vesicles, coalesced together (Figure 6). Still higher toxin concentrations resulted in formation of micelles, which were too small to be observed with the fluorescence microscope. A similar effect was observed in the presence of the nonionic detergent Triton X-100: at a low concentration the detergent altered the morphology of the GUV, which coalesced into clusters of smaller vesicles; at higher concentrations the vesicles were broken up into micelles or toxin−lipid aggregates invisible to the microscope. These results strongly suggest that Cyt1A acts in a detergent-like manner, rather than as a pore former. If the latter was the case, no toxin-induced changes in the size or morphology of the model membranes would be expected in the state of osmotic equilibrium between the interior and exterior of the vesicles: the membrane would be leaky, but there would be no reason for it to disintegrate.

Many antimicrobial peptides seem to act in a detergent-like manner: for example, apomyoglobulin 56−131 peptide (*25*), human antimicrobial peptide LL-37 (*26*), surfactin (*27*), or melittin (*28*). It should be noted that these peptides' mode of action is highly dependent on the nature of the lipid and the peptide concentration. The latter suggests that a threshold of peptide concentration needs to be reached before the membranes are damaged (*25, 26*). Electrostatic interactions were shown to play an important role in the peptide aggregation on the membrane surface (*28*). Interestingly, these functional characteristics are shared with Cyt1A: A threshold concentration needed to be reached before the faster diffusers appeared in our FPR experiments (Figures 4 and 5), before a fluorescent dye was released from the vesicles (*9*), and before the insect Malpighian tubules were compromised (*29*). The importance of electrostatics in the Cyt1A interaction with lipid membranes, first recognized by Haider and Ellar (*30*), is confirmed here in the experiments with the ionic strength (Figure 3A).

In conclusion, the FPR and fluorescence microscopy data give strong support to the detergent model of the Cyt1A action, and the other presented results are consistent with that model. However, the detergent model cannot easily accommodate some important features of the Cyt1A action, namely, the toxin's specificity for certain insects and its high affinity for unsaturated lipids. Despite this shortcoming, we are convinced that our biophysical experiments with simple model systems will complement the available biological and toxicological data and will contribute to the ultimate elucidation of the Cyt1A's mode of action in the much more complex environment in vivo.

REFERENCES

1. Knowles, B. H., and Dow, J. A. T. (1993) The crystal delta-endotoxin of *Bacillus thuringiensis*: models for their mechanism of action on the insect gut, *BioEssays 15*, 469−476.
2. Li, J., Derbyshire, D. J., Promdonkoy, B., and Ellar, D. J. (2001) Structural implications for the transformation of the *Bacillus thuringiensis* delta-endotoxins from water-soluble to membrane-inserted forms, *Biochem. Soc. Trans. 29*, 571−577.
3. Knowles, B. H., and Ellar, D. J. (1987) Colloid-osmotic lysis is general feature of the mechanism of action of *Bacillus thuringiensis* delta-endotoxins with different insect specificity, *Biochim. Biophys. Acta 924*, 509−518.
4. Thomas, W. E., and Ellar, D. J. (1983) *Bacillus thuringiensis* var. *israelensis* crystal delta-endotoxin: effects on insect and mammalian cells in vitro and in vivo, *J. Cell Sci. 60*, 181−197.
5. Knowles, B. H., Blatt, M. R., Tester, M., Horsnell, J. M., Carroll, J., Menestrina, G., and Ellar, D. J. (1989) A cytolytic delta-endotoxin from *Bacillus thuringiensis* var. *israelensis* forms cation-selective channels in planar lipid bilayers, *FEBS Lett. 244*, 259−262.
6. Butko, P. (2003) Cytolytic toxin Cyt1A and its mechanism of membrane damage: data and hypotheses, *Appl. Environ. Microbiol. 69*, 2415−2422.
7. Thomas, W. E., and Ellar, D. J. (1983) Mechanism of action of *Bacillus thuringiensis* var. *israelensis* insecticidal delta-endotoxin, *FEBS Lett. 154*, 362−368.
8. Butko, P., Huang, F., Pusztai-Carey, M., and Surewicz, W. K. (1997) Interaction of the delta-endotoxin CytA from *Bacillus thuringiensis* var. *israelensis* with lipid membranes, *Biochemistry 36*, 12862−12868.
9. Butko, P., Huang, F., Pusztai-Carey, M., and Surewicz, W. K. (1996) Membrane permeabilization induced by cytolytic delta-endotoxin CytA from *Bacillus thuringiensis* var. *israelensis*, *Biochemistry 35*, 11355−11360.
10. Chilcott, C. N., and Ellar, D. J. (1988) Comparative toxicity of *Bacillus thuringiensis* var. *israelensis* crystal proteins in vivo and in vitro, *J. Gen. Microbiol. 134* (Part 9), 2551−2558.
11. Moscho, A., Orwar, O., Chiu, D. T., Modi, B. P., and Zare, R. N. (1996) Rapid preparation of giant unilamellar vesicles, *Proc. Natl. Acad. Sci. U.S.A. 93*, 11443−11447.
12. Butko, P., He, J., and Nicholls, P. (1992) Valinomycin modifies phosphorescence quenching in cytochrome *c* oxidase, *Biochem. Biophys. Res. Commun. 189*, 1477−1483.
13. Lakowicz, J. R. (1999) *Principles of fluorescence spectroscopy*, Kluwer Academic/Plenum Publishers, New York.
14. Promdonkoy, B., and Ellar, D. J. (2003) Investigation of the pore-forming mechanism of a cytolytic delta-endotoxin from *Bacillus thuringiensis*, *Biochem. J. 374*, 255−259.
15. Fong, B., Stryjewski, W., and Russo, P. S. (2001) On the use of pattern fluorescence photobleaching recovery with modulation

detection to obtain colloidal size distributions, *J. Colloid Interface Sci. 239*, 374−379.
16. Agirre, A., Barco, A., Carrasco, L., and Nieva, J. L. (2002) Viroporin-mediated membrane permeabilization. Pore formation by nonstructural poliovirus 2B protein, *J. Biol. Chem. 277*, 40434−40441.
17. Koni, P. A., and Ellar, D. J. (1994) Biochemical characterization of *Bacillus thuringiensis* cytolytic delta-endotoxins, *Microbiology 140*, 1869−1880.
18. Ward, E. S., Ellar, D. J., and Chilcott, C. N. (1988) Single amino acid changes in the *Bacillus thuringiensis* var. *israelensis* delta-endotoxin affect the toxicity and expression of the protein, *J. Mol. Biol. 202*, 527−535.
19. Du, J., Knowles, B. H., Li, J., and Ellar, D. J. (1999) Biochemical characterization of *Bacillus thuringiensis* cytolytic toxins in association with phospholipid bilayer, *Biochem. J. 338*, 185−193.
20. Promdonkoy, B., and Ellar, D. J. (2000) Membrane pore architecture of a cytolytic toxin from *Bacillus thuringiensis*, *Biochem. J. 350*, 275−282.
21. Walker, B., Krishnasastry, M., Zorn, L., and Bayley, H. (1992) Assembly of oligomeric membrane pore formed by staphylococcal alpha-hemolysin examined by truncation mutagenesis, *J. Biol. Chem. 267*, 21782−21786.
22. Manceva, S. D., Pusztai-Carey, M., and Butko, P. (2004) Effect of pH and ionic strength on the cytolytic toxin Cyt1A: a fluorescence spectroscopy study, *Biochim. Biophys. Acta 1699*, 123−130.
23. Shai, Y. (1995) Molecular recognition between membrane-spanning polypeptides, *Trends Biochem. Sci. 20*, 460−464.
24. Shepard, L. A., Shatursky, O., Johnson, A. E., and Tweten, R. K. (2000) The mechanism of pore assembly for a cholesterol-dependent cytolysin: formation of a large prepore complex precedes the insertion of the transmembrane beta-hairpins, *Biochemistry 39*, 10284−10293.
25. Mak, P., Szewczyk, A., Mickowska, B., Kicinska, A., and Dubin, A. (2001) Effect of antimicrobial apomyoglobin 56−131 peptide on liposomes and planar lipid bilayer membranes, *Int. J. Antimicrob. Agents 17*, 137−142.
26. Oren, Z., Lerman, J. C., Gudmundsson, G. H., Agerberth, B., and Shai, Y. (1999) Structure and organization of the human antimicrobial peptide LL-37 in phospholipid membranes: relevance to the molecular basis for its non-cell-selective activity, *Biochem. J. 341* (Part 3), 501−513.
27. Heerklotz, H., and Seelig, J. (2001) Detergent-like action of the antibiotic peptide surfactin on lipid membranes, *Biophys. J. 81*, 1547−1554.
28. Ladokhin, A. S., and White, S. H. (2001) "Detergent-like" permeabilization of anionic lipid vesicles by melittin, *Biochim. Biophys. Acta 1514*, 253−260.
29. Maddrell, S. H., Overton, J. A., Ellar, D. J., and Knowles, B. H. (1989) Action of activated 27,000 Mr toxin from *Bacillus thuringiensis* var. *israelensis* on Malpighian tubules of the insect, *Rhodinius prolixis*, *J. Cell Sci. 94*, 601−608.
30. Haider, M. Z., and Ellar, D. J. (1989) Mechanism of action of *Bacillus thuringiensis* insecticidal delta-endotoxin: interaction with phospholipid vesicles, *Biochim. Biophys. Acta 978*, 216−222.

BI048493Y